Modeling the Solids Conveying Zone of a Novel Extruder

Mingyin Jia, Kejian Wang, Ping Xue, Fuhua Zhu

Institute of Plastics Machinery and Plastics Engineering, Beijing University of Chemical Technology, P.O. Box 60, Beijing, China 100029

Received 4 June 2007; accepted 10 August 2007
DOI 10.1002/app.27237
Published online 30 October 2007 in Wiley InterScience (www.interscience.wiley.com).

ABSTRACT: On the basis of the theory of relative motions, a novel nested screw extruder was invented in which one rotating outer screw acted as the barrel for an inner screw; the combination of the outer screw and outer barrel was the other extrusion system. It was realized that centrifugal force resulted in the difference between the forces acting on the solids by the screw and by the barrel, which further compacted the solid pellet or powder. These factors benefited the frictional drag of solids and the early melting. This was consistent with the fact that the solids conveying flow rate increased greatly when the barrel and screw rotated oppositely at the same time. Thus, centrifugal force and material compressibility were significant in the feeding zone. A mathematical model was developed to calculate the output, pressure, and velocity of the solids in the screw down-channel with consideration of the centrifugal force and material compressibility. The predicted pressure distribution and output were better than those by previous models in fitting the experimental data. The simulations revealed that the maximum traction angle was close to 90° − the helix angle for maximum output in contrast to the maximum traction angle of 90° predicted by the Darnell–Mol theory. © 2007 Wiley Periodicals, Inc. J Appl Polym Sci 107: 1990–1999, 2008

Key words: extrusion; modeling; simulations; theory

INTRODUCTION

Extrusion is one of the basic and convenient processing elements used to melt polymers for further molding. The zone from the feeding inlet to the point at which the solid–barrel interface temperature arrives at the polymer melting point is in general defined as the solids conveying zone. The conveying of solids exerts an important influence on the performance of the extruder. However, in comparison with the great amount of research on melt conveying in screw extruders, much less attention has been paid to the conveying of solids because of the complexity of the solids conveying process.

The earliest solids conveying theory was established by Darnell and Mol[1] in 1965, and it was based on solid static friction. In 1970, Chung[2] put forward a viscosity traction theory in which a solid bed was forwarded by the slip of a melt layer between a solid plug and the surface of the metal. In 1971, Tedder[3] analyzed the motion of pellets, using the energy-balance theory and virtual displacement principle. In 1972, Broyer and Tadmor[4] modified the Darnell–Mol model, considering the effects of a screw helix. However, the density variation was not considered, and the velocity of the solids along the screw channel was assumed to be constant in the aforementioned theories. In fact, it is a gradual transition process from a granular state to a compact state, not instant formation into a so-called solid bed or solid plug. Fang et al.[5] observed such a process in a transparent extruder and developed the nonplug solids conveying theory, using a finite element analysis model.[5] Unfortunately, the aforementioned research did not take into account inertial forces under the assumption of a stationary screw and a rotating barrel. Thus, their models could not well explain the origin of pressure buildup and the effect of centrifugal force on the conveying of solids. Lovegrove and Williams[6] studied the effects of gravity forces and centrifugal force on the pressure initial setup in the feeding section of the extruder. The model predicted that centrifugal force would have a strong effect on the pressure at the first turns along the screw, especially when the screw speed was high. However, the contributions of centrifugal force and gravity were simply considered in a pressure differential equation. Their effects on the conveying of solids are detailed here.

In this study, a novel screw extruder was introduced in which one rotating outer screw, one stationary or oppositely rotating inner screw, and one stationary outer barrel were nested as two extrusion systems. In developing the novel extruder, we perceived that inertial forces caused by the rotating screw possibly had a strong effect on the feeding, pressure, and velocity of the solid in the solids conveying zone. Thus, this article provides solid motion

Correspondence to: P. Xue (johnmy2008@sohu.com).

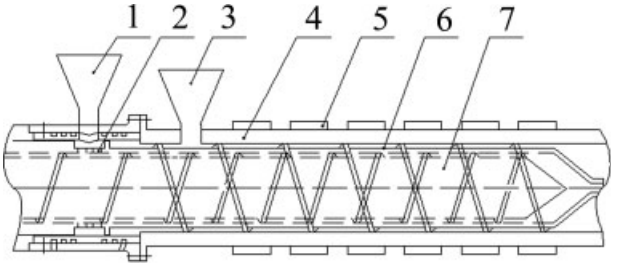

Figure 1 Schematic diagram of the novel extruder: (1) first hopper, (2) entrance hole, (3) second hopper, (4) barrel, (5) heater, (6) outer screw, and (7) inner screw.

analyses by considering centrifugal force and solid compressibility in the solids conveying zone of the novel extruder. On the basis of the physical image, a numerical model was set up, and an analytical solution was obtained. The output and effect of the centrifugal force on the feeding, traction angle, and pressure distribution in the special case of the rotating screw and oppositely rotating internal barrel were examined.

NOVEL NESTED EXTRUDER

A general extruder is designed to include a stationary barrel and a rotating screw. It is well known that much more energy is used by general single-screw extruders than is required to melt solid plastic. In many experiments, it has been found that the consumed energy is more than twice that theoretically needed. However, according to the theory of relative motion, the relative revolution between a screw and a barrel can be produced either by the coupling of a stationary screw and a rotating barrel or by the coupling of a rotating screw and an oppositely rotating barrel to convey materials. Thus, a high relative velocity has been expected to save energy. For instance, as early as 1979, Klein and Klein[7] invented a solid-draining screw extruder that included a rotating outer screw and a stationary inner screw segment mounted on the breaker plate or the perforated metal plate in the die. In 1992, Campbell et al.[8] designed a special screw extruder to study the drag flow of melt conveying. The barrel, screw core, and screw flights could all rotate independently or simultaneously in pairs. In 2003, Sarioglu and coworkers[9,10] introduced a Conex extruder to extrude two layers in one extruder. Several concentric tapered rotors were nested to act as multiple extruders.

In this study, another novel extruder was introduced. The key was that the outer screw and inner screw were nested. The inner screw remained stationary or rotated oppositely to the outer screw. The rotating outer screw was used as the barrel of the inner screw. Besides, the outer screw rotated against the stationary barrel in the normal form. The structure is shown in Figures 1 and 2. The outer screw and inner screw were driven by two different motors and were fed through two different hoppers. On the one hand, double-layer products could be extruded by the novel screw extruder. On the other hand, the total output was equal to that of two single-screw extruders when the outer screw and inner screw extruded the same materials.

Klein and Klein[7] used only a short-section inner screw with respect to the outer screw just for solid draining in their extruder. In contrast, one inner screw was almost as long as the outer one in this novel extruder. A double layer could also be coextruded. Besides, the Conex extruder consisted of conical static parts and conical rotating parts; this is different from common screws and more difficult to manufacture, assemble, and maintain. The present novel extruder compounded two single-screw extruders, this being easier to do. Additionally, the inner screw could adequately use the heat from the outer screw to melt plastic. Thus, it had higher efficiency and large output, and little energy was expended.

PHYSICAL IMAGE AND MATHEMATICAL MODEL

Basic assumptions

1. The coefficients of frictions and the temperature of the pellets are assumed to be constant.
2. The ratio of the normal stress to the axial (moveable direction) stress is constant. It is independent of the position; that is, the stress is constantly distributed.

Figure 2 Photograph of the novel screw extruder.

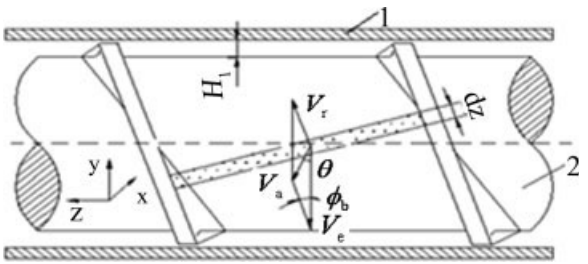

Figure 3 Velocity diagram of the solids conveying zone: (1) barrel and (2) screw.

3. The material density, normal stress, and axial stress change only along the moving direction of the material.
4. The shape of the channel is rectangular. The channel depth of the solids conveying zone is constant.

Motion analysis

Figure 3 shows the velocity diagram of the solids in the case of a rotating screw and an oppositely rotating barrel in the solids conveying zone. The screw is selected as a moving reference system, the barrel is a static reference system, and the solid is moving circularly while turning around the axis of the convected motion. $\vec{V}_r$ is the relative velocity, $\vec{V}_e$ is the convected velocity, and $\vec{V}_a$ is the absolute velocity. The relations are as follows:

$$\vec{V}_a = \vec{V}_r + \vec{V}_e \tag{1}$$

$$V_e = \pi D_b (n_1 + n_2) \tag{2}$$

where D_b is the diameter of the barrel and n is the rotational speed. Subscripts 1 and 2 indicate the screw and barrel, respectively, just as subscripts s and b do.

For calculating the volumetric flow rate (Q_s), the axial velocity (V) and vertical cross section area (A) should be calculated. The relations can be written as follows:

$$Q_s = VA, \quad V = V_a \tan\phi_b \tag{3}$$

$$A = \frac{\pi}{4}(D_b^2 - D_s^2) - \frac{eH_1}{\sin\phi} \tag{4}$$

where D_s is the root diameter of the screw, e is the width of the screw flight, ϕ_b is the helix angle of the barrel, $\bar{\phi}$ is the average helix angle, and H_1 is the channel depth of the solids conveying zone.

Thus, Q_s in the case of a rotating screw and an oppositely rotating barrel can be calculated with the following equation:

$$Q_s = \pi^2 D_b (n_1 + n_2) H_1 (D_b - H_1) \frac{\sin\theta \tan\phi_b}{\sin(\theta + \phi_b)} \left(\frac{\overline{W}}{\overline{W} + e}\right) \tag{5}$$

where θ is the traction angle and $\overline{W}$ is the average channel width.

The relative rotation of the screw greatly increases when the screw and the internal barrel rotate oppositely at the same time. Thus, the total volumetric flow rate almost equals the volumetric flow rate of two single-screw extruders with the same screw geometrical variables and rotational speeds n_1 and n_2, respectively.

Acceleration analysis

Figure 4 shows the acceleration analysis under the condition in which the screw is selected as the moving reference system and the barrel is the static reference system. When convected motion is treated as around the axis, the Coriolis acceleration (a_c) of the moving solids consists of two parts. The first is caused by the position variation of the coincidence point between the screw and barrel. The second is caused by the velocity direction variation with the rotating screw.

a_c can be calculated as follows:

$$a_c = \frac{2V_b^2}{R} \frac{\sin\theta \cos\phi_b}{\sin(\theta + \phi_b)} \tag{6}$$

where V_b is the axial velocity of the barrel and R is the radial radius of outer diameter of the screw. The absolute acceleration (a_a) is the combination of the relative acceleration (a_r), convicted acceleration (a_e), and a_c:

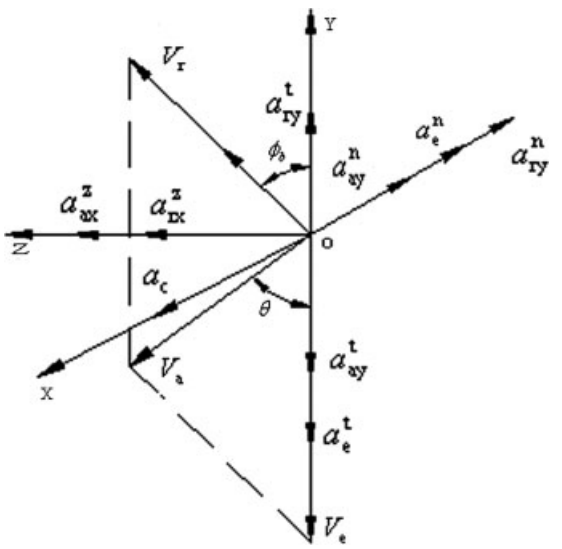

Figure 4 Diagram of solid acceleration in the solids conveying zone.

$$\vec{a}_a = \vec{a}_e + \vec{a}_r + \vec{a}_c \tag{7}$$

V_r, V_e, and V_a all can be decomposed into the normal velocity, tangential velocity, and axial velocity along axis X, axis Y, and axis Z, respectively. Superscripts n, t, and z indicate normal, tangential, and axial directions, respectively. That is, normal acceleration a^n_{ay} in the direction of axis X includes a^n_{ry}, a^n_e, and a_c. Tangential acceleration a^t_{ay} in the direction of axis Y includes a^t_{ry} and a^t_e. Axial acceleration a^z_{az} in the direction of axis Z refers to a^z_{rz}. Equations (8)–(10) can be obtained from eq. (7).

Here the radial radius is considered the outer diameter of the screw for simplification because the channel depth is far lower than the diameter. Normal acceleration reflects the magnitude of the forces produced by the screw and barrel, and this influences the compacting degree of the pellets in the normal direction, which is

$$a^n_{ay} = \frac{V_b^2}{R}\left(\frac{\sin\phi_b\cos\theta}{\sin(\theta+\phi_b)}\right)^2 \tag{8}$$

Tangential acceleration influences the compacting degree of the pellets in the tangential direction. Because $a^t_{ay} = -a^t_{ry} + a^t_e$ and $a^t_e = 0$, thus

$$a^t_{ay} = -a^t_{ry} \tag{9}$$

Axial acceleration changes the axial velocity and displacement, influencing the degree of the solids in the axial direction. Thus,

$$a^z_{ax} = a^z_{rx} \tag{10}$$

On the basis of eq. (8), normal acceleration a^n_{ay} is positive no matter what the values of θ and ϕ_b are. This indicates that the force acting on the solids by the barrel is larger than that by the screw in the solids conveying zone. The higher the value is of a^n_{ry}, the more closely the solids compact. Therefore, increasing the normal force of the barrel on the material and reducing the normal force of the screw both favor the conveying of solids by increasing the friction coefficient of the barrel/material and reducing the friction coefficient of the screw/material, respectively. Equation (8) also indicates that the important variable affecting normal acceleration is the traction angle when the helix angle is invariable.

If we suppose that the normal force of the barrel acting on the solid is N_1, the normal force of the screw acting on the solid is N_2, and the mass of the solids is $\rho d\bar{z} H_1 \overline{W}$, we can obtain the following:

$$N_1 - N_2 = \rho d\bar{z} H_1 \overline{W} a^n_{ay} \tag{11}$$

where ρ is the density of the solids and $d\bar{z}$ is the average down-channel differential increment.

The key factors that affect the friction force are the friction coefficient and normal force. From eq. (11), it is concluded that the conveying of solids can still be carried out even though the friction coefficient between the barrel and solids is smaller than the friction coefficient between the screw and solids. This case was supported by Tedder[3] in his experiments.

Mathematical model

A down-channel differential element is depicted in Figure 3. The continuity equation can be determined for the solids by the consideration of the conservation of mass of the differential element. The equation is

$$\frac{\partial\rho}{\partial t} + v\frac{\partial\rho}{\partial z} + \rho\frac{\partial v}{\partial z} = 0 \tag{12}$$

where ρ is the material density at pressure P, t is the time, v is the velocity, and z is down-channel distance.

Chung's[11] experimental work indicated that the variation of the material density could be expressed by an empirical equation of the following form:[11]

$$\rho = \rho_m - (\rho_m - \rho)\cdot e^{-C_0 p} \tag{13}$$

where ρ_m is the density under utmost pressure, ρ_a is the bulk density at the atmospheric pressure, p is the pressure, and C_0 is a constant.

Substituting eq. (13) into eq. (12) leads the continuum equation to be expressed as follows:

$$\frac{\partial\rho}{\partial t} + v\frac{\partial\rho}{\partial z} + \frac{1}{C_0}\left(\frac{\rho_m}{\rho_m - \rho_a}e^{C_0 p} - 1\right)\frac{\partial v}{\partial z} = 0 \tag{14}$$

The kinematic equation can be determined by the application of force and torque balance to a differential element of the solids in the down-channel direction. The equation is given as follows:

$$\frac{\partial p}{\partial z} + K_f p + \rho\left(v\frac{\partial v}{\partial z} + \frac{\partial v}{\partial t} + K_b v^2\right) = 0 \tag{15}$$

where

$$K_b = \frac{f_b}{R}(\sin\phi_b\cot\theta)^2[f_s\sin(\theta+\phi_b) - \cos(\theta+\phi_b)] \tag{16}$$

$$K_f = \frac{f_b K}{H_1}\left[\frac{f_s}{f_b}\frac{\overline{W}+2H_1}{\overline{W}} + f_s\sin(\theta+\phi_b) - \cos(\theta+\phi_b)\right] \tag{17}$$

Constant K refers to the ratio of the normal stress to the axial (the moveable direction) stress.[12] To solve the mathematical model, eqs. (14) and (15)

TABLE I
Geometrical Parameters of the Solids Conveying Zone of the Novel Extruder

	Outer screw	Inner screw
Diameter, D (mm)	50	32
Channel depth, H_1 (mm)	5	4.5
Helix angle, ϕ_b	11° 30′	17° 40′
Length–diameter ratio	20	30
Width of helix channel, W (mm)	15	27.3
Screw pitch, S (mm)	32	32
Width of helix flight (mm)	5	3.2
Design length of solids conveying zone, L	8S	8D

were converted to be dimensionless and linear, as mentioned in ref. 12. If $\bar{\rho}$, $\bar{p}$, $\bar{v}$, and $\bar{t}$ are the dimensionless characteristic parameters of the density, pressure, velocity, and time, respectively, L is the length of the solids conveying zone, and v_0 is the inlet velocity, we can obtain the following:

$$p = \bar{p}(1 + p^*); \quad \rho = \bar{\rho}(1 + \rho^*); \quad v = \bar{v}(1 + v^*); \quad t = \bar{t}\ t^*; \quad z = Lz^* \tag{18}$$

Dimensionless boundary conditions can be shown as follows:

$$v^*|_{z^*=0} = \frac{v(z,t)|_{z=0}}{\bar{v}} - 1 = v_0^*(t) = v_0^* \tag{19}$$

$$p^*|_{z^*=0} = \frac{p(z,t)|_{z=0}}{\bar{p}} - 1 = p_0^*(t) = p_0^* \tag{20}$$

Using the ultimate value theory in Laplace transform, we can express the approximate analytical solutions of the pressure and velocity as the following equations. More details on the solving method can be found in ref. 12:

$$P(z) = p_0 \exp\left(\frac{-\beta_1 Z}{L}\right) \tag{21}$$

$$V(z) = v_0 - \frac{C_0 v_0(\rho_m - \bar{\rho})(\bar{p} - p_0)}{\bar{\rho}}(e^{-\beta_1 Z} - 1) \tag{22}$$

where

$$\beta_1 = \frac{\bar{\rho}e^{C_0\bar{p}}(\bar{p}LK_f + \gamma^2 LK_b\rho_m\bar{v}^2)}{\bar{p}[\bar{\rho}e^{C_0\bar{p}} - \gamma^2\rho_m\bar{v}^2C_0(\rho_m - \rho_a)]} \tag{23}$$

$$\bar{p} = \frac{1}{Z}\int_0^z p_0 e^{-\frac{\beta_1 z}{L}} dz \tag{24}$$

RESULTS AND DISCUSSION

The basic geometrical parameters of the novel extruder are presented in Table I. High-density polyethylene (HDPE; 5000S type) was used in the experiments. HDPE was supplied by Beijing Yanshan Plant (Beijing, China). The densities of HDPE in the utmost pressure and in the atmospheric pressure were 520 and 860 kg/m^3, respectively. The samples were extruded at 170, 186, 190, 195, 193, 195, and 192°C from the hopper to the die. In the tests, a pressure sensor was installed at the end of the solids conveying zone of the outer screw on the experimental extruder. p_0 is the pressure at the bottom of the hopper, and its value is approximately 0.098 MPa.

Output and screw torque

The output of the inner screw and the electric currents at different relative rotating speeds of the outer screw and inner screw are listed in Table II. The out-

TABLE II
Experimental Data and Calculated Data on the Novel Extruder

					Calculated output of the inner screw by the model (kg/h)		
n_1 (rpm)	n_2 (rpm)	I_1 (A)	I_2 (A)	Experimental output of the inner screw (kg/h)	f_1 = 0.30, f_2 = 0.30	f_1 = 0.30, f_2 = 0.25	f_1 = 0.35, f_2 = 0.30
8	2	11.5	6.7	1.543	1.980	5.702	4.955
8	4	12.1	7.3	1.747	2.377	6.843	5.945
8	6	12.6	7.7	2.053	2.774	7.984	6.938
8	8	13.0	8.6	2.359	2.980	9.124	7.923
10	2	11.6	6.6	1.726	2.377	6.843	5.945
12	2	12.7	7.3	2.012	2.774	7.984	6.938
14	2	13.7	8.0	2.298	2.980	9.124	7.923
14	3	13.8	8.6	3.170	3.364	9.694	8.424

n_1 and n_2 are the outer and inner screw rotational speeds, respectively; I_1 and I_2 are the electric currents of the outer and inner screw, respectively; and f_1 and f_2 are the friction coefficients between the barrel and material and between the screw and material, respectively.

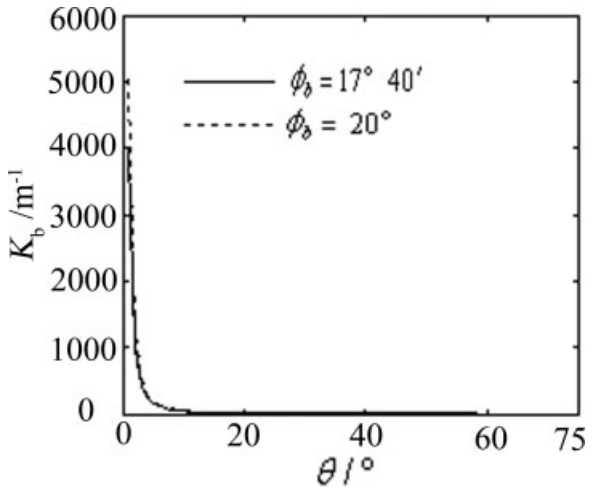

Figure 5 Relationship between K_b and θ.

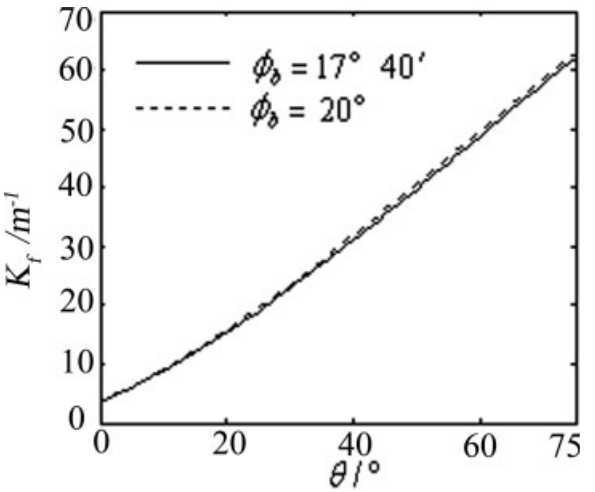

Figure 6 Relationship between K_f and θ.

put of the inner extrusion system increases greatly with the rotating inner screw and oppositely rotating outer screw at the same time even though the inner screw rotating speed is as low as 2 rpm. The output of the inner extrusion system also increases when the outer screw speed is increased and the inner screw speed is kept constant. Moreover, the calculated outputs for the combination of 0.25/0.30 or the combination of 0.30/0.35 of solid friction coefficients against the inner screw/outer screw are much higher than those of the experimental data and calculated data for 0.30/0.30. Thus, it can be concluded that the combination of 0.30/0.30 of the solid friction coefficients against the inner screw/outer screw seems closer to the actual value. As expected, the calculated output increases when the inner screw/solids friction coefficient is reduced or the outer screw/solids friction coefficient is increased; the former is more effective.

The variation of the electric current reflects the change in the screw torque because the output torque of a three-phase induction motor is proportional to the electric current. The outer screw torque increases with the enhancement of the inner screw speed because of the opposite torque exerted on the outer screw by the inner screw when the outer screw speed is kept constant. This is similar to the increment in the inner screw torque with the enhancement of the outer screw speed because of the increase in the relative speed of the inner screw.

Effect of centrifugal force on feeding

In terms of eqs. (16) and (17), coefficients K_b and K_f indicate the effects of centrifugal force and friction forces on the conveying of solids, respectively. Figures 5 and 6 show the relationship between the two coefficients and traction angle. From Figure 5, it can be seen that K_b is infinite when the traction angle is close to zero. In this case, the centrifugal force reaches the maximum, and solids only rotate around the screw without being conveyed forward. The setup pressure is almost completely used to compress solids, corresponding to the maximum density and maximum pressure. Coefficient K_b decreases with increasing traction angle because of low tangential velocity and low centrifugal force. From eq. (17) and Figure 6, it can be found that K_f increases with the rise of the traction angle because of the high axial velocity and high friction forces between the solids and screw. It also can be found from the figures that the effect of the helix angle on K_b and K_f is not obvious.

Materials were fed into the inner extrusion system through the double-row, wedge-shaped holes of the outer screw. The shape of the holes is shown in Figure 7. The feeding manner of the outer extrusion was the same as that of the general single-screw extruder. The experiments were made under the following three cases. The first case was that the outer screw rotated while the inner screw was kept stationary. The second case was that the outer screw was kept stationary while the inner screw rotated.

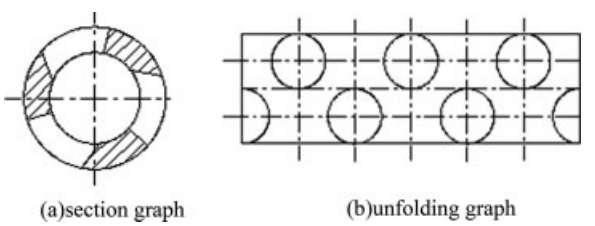

Figure 7 Feeding holes of inner extrusion system.

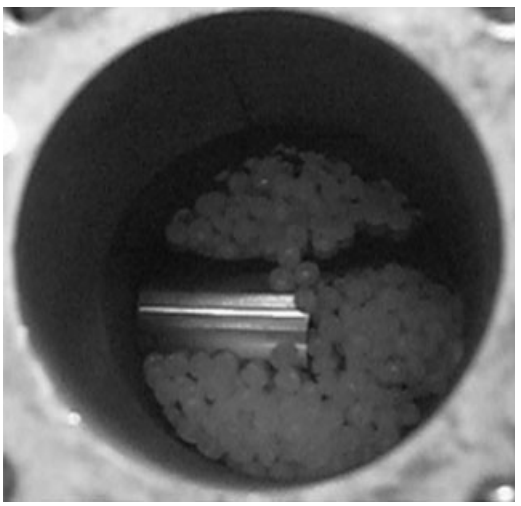

Figure 8 Photograph of the feeding of the inner screw with the rotating outer screw and stationary inner screw.

The last case was that the outer screw and inner screw both rotated oppositely.

In the first case, it was observed that the solids only rotated with the rotating outer screw. Only a small number of plastics pellets were fed into the inner extrusion system, as shown in Figure 8. The forces exerted on the solids included the pressure force, outer screw friction force, inner screw friction force, inner screw flight additional force, and outer screw centripetal force. However, there was no centrifugal force on the solids when the inner screw was stationary, and this made the outer screw friction force higher than that of the inner screw friction force. The common solids friction conveying mechanism was broken down. Thus, the solids in the feeding zone of the inner screw could not effectively be conveyed in this case.

The second case was the same as the general single screw. The solids were conveyed with inner screw centrifugal force, friction forces, and so on. The normal acceleration induced the force of the inner screw acting on the solids, which was always higher than that of the outer screw acting on the solids.

In the third case, it was observed that the solids in the feeding zone of the inner screw were conveyed quite quickly even with a low inner screw speed, as shown in Figure 9. The forces exerted on the solids in this case included the inner screw centrifugal force and outer screw centripetal force, in addition to the friction forces and pressure forces. The effect of the centrifugal force is stronger than that of the centripetal force. Thus, it was further supposed that the force of the inner screw acting on the solids was higher than that of the outer screw acting on the solids due to centrifugal force.

Traction angle

According to Figure 3, the following relationship between V_r and V_e can hold:

$$V_r = \frac{V_e \sin\theta}{\sin(\phi_b + \theta)} \tag{25}$$

Thus, the traction angle can be obtained from eqs. (21), (22), and (25) as follows:

$$\cot\theta = \frac{p_0\bar{\rho}}{[p_0\bar{\rho} - C_0(\rho_m - \bar{\rho})(\bar{p} - p_0)(p - p_0)]\sin\phi_b\cos\phi_b} - \cot\phi_b \tag{26}$$

Pressure increases as solids are gradually compacted in the solids conveying process, which results in the reduction of the velocity of the solids. Therefore, the traction angle changes along the direction of the screw channel, as expressed in eq. (26). Figure 10 shows the relationship between the traction angle and pressure of the inner screw with various initial pressures. The traction angle decreases with the increment of pressure. This is similar to the simulated results in ref. 11. In addition, the traction angle is close to zero at the maximum pressure corresponding to the end of solids conveying, and the traction angle reaches its maximum at the beginning of the solids conveying zone corresponding to zero pressure.

It is worth mentioning that the maximum volumetric flow rate is obtained when the traction angle is 90° by the Darnell–Mol theory, whereas the maximum traction angle is almost equal to 90° − 17° 40′ by this model. The difference mainly results from the centrifugal force considered in the modeling. Figure 11 shows an orthogonal complementary relation

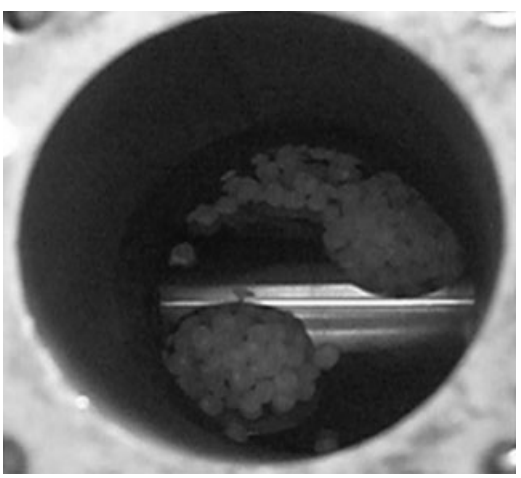

Figure 9 Photograph of the feeding of the inner screw with the rotating outer screw and oppositely rotating inner screw.

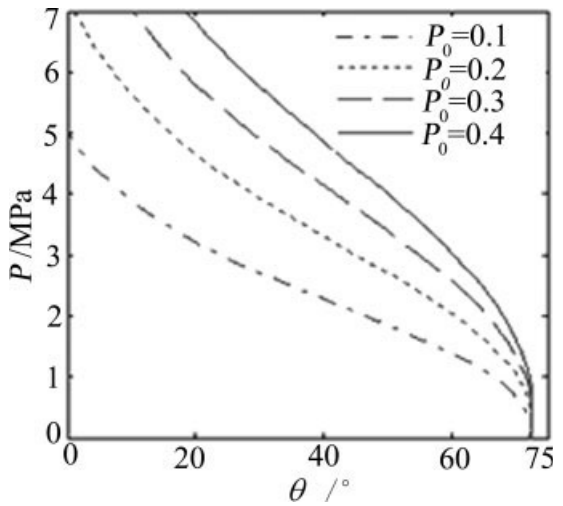

Figure 10 Relationship between the traction angle (θ) and pressure (P) of the inner screw.

between the maximum traction angle and the helix angle, namely, $\theta_{max} = 90^\circ - \phi_b$.

Figure 12 shows the effects of the geometrical parameters and inner screw rotational speed on the maximum traction angle. The maximum traction angle increases sharply until H_1/D arrives at 0.15 and then increases slowly. It can be concluded that there is an optimal channel depth for getting the maximum traction angle. It can also be found that the higher the inner screw rotational speed is, the lower the maximum of the traction angle is. This may be due to the fact that centrifugal force increases with a high inner screw rotational speed and the solids are compressed along the normal direction.

Pressure distribution

Equation (21) indicates that pressure distribution in the solids conveying zone is not only a function of

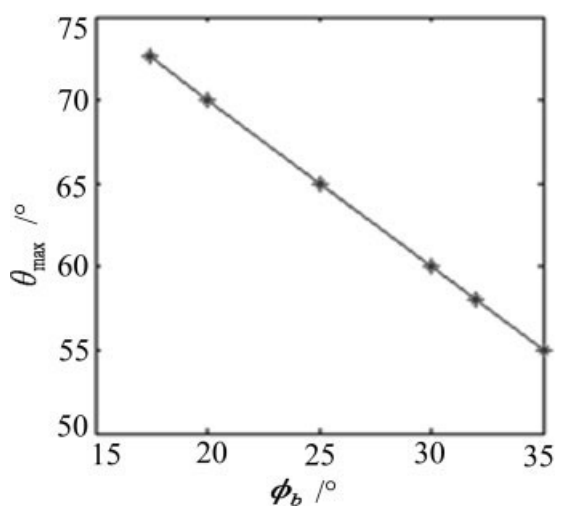

Figure 11 Relationship between the helix angle (ϕ_b) and the limit traction angle (θ_{max}) of the inner screw.

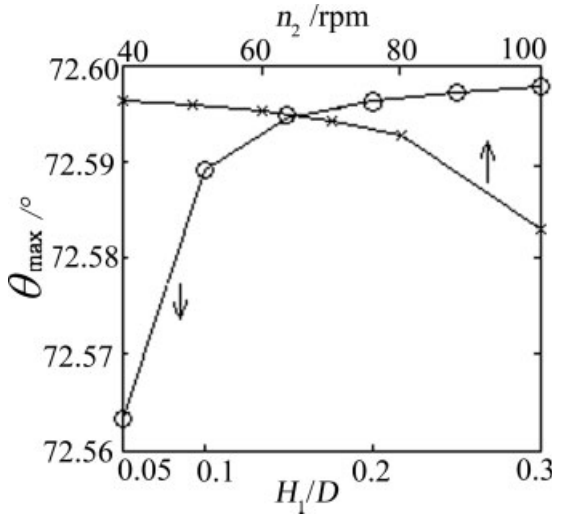

Figure 12 Effects of H_1/D and the inner screw rotational speed (n_2) on the limit traction angle (θ_{max}).

the friction coefficient, density, and geometrical parameters of the screw but also a function of the velocity. This cannot be explained by the previous Darnell–Mol theory[1] and Sun's analysis.[13] In our opinions, the solids are compressed gradually and the density of the solids changes along the conveying length.

Figure 13 shows the predicted pressure distributions of the inner screw and outer screw in the solids conveying zone. The predicted results are in contrast to the measured data and the data calculated by the Darnell–Mol theory. It can be seen that the predicted

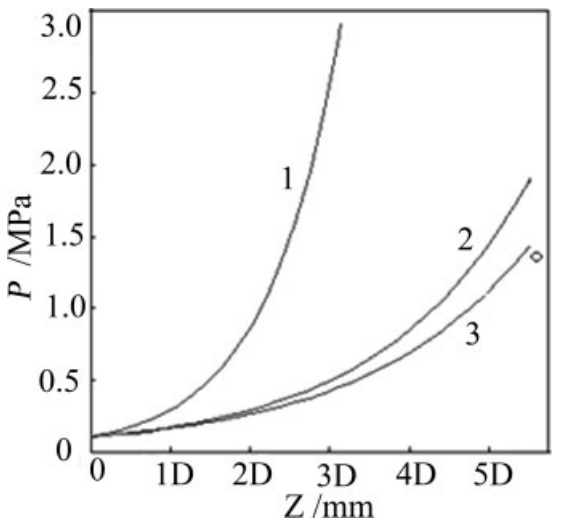

Figure 13 Pressure distributions along the solids conveying zone: (1) pressure of the outer screw by the Darnell–Mol theory (n_1 = 60 rpm), (2) pressure of the inner screw by the model (n_1 = 60 rpm, n_2 = 60 rpm), and (3) pressure of the outer screw by the model (n_1 = 60 rpm). The circle indicates the experimental data for the outer screw.

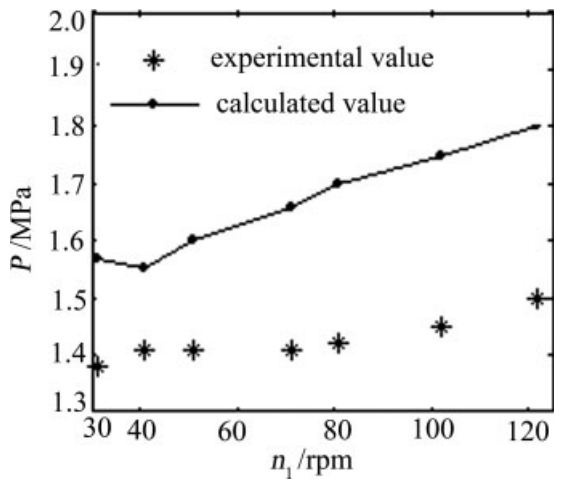

Figure 14 Relationship between the outer screw rotating speed (n_1) and limit pressure (P).

pressure curves obey Fick's law. The pressure distribution in the case of oppositely rotating inner and outer screws is higher than that of a stationary barrel and a rotating outer screw. The former can be explained by the increased velocity and inertial acceleration of the solids, which subsequently has a strong effect on the density and results in an increment of pressure. Curve 1 in Figure 13 presents the pressure distribution in the case of a rotating outer screw and a stationary barrel calculated by the Darnell–Mol model under the same conditions used for curve 3 by this model. The pressure by the Darnell–Mol theory is much higher than the one by this model because the density of the solids is assumed to be invariable in the Darnell–Mol theory, which is not the actual case. One experimental value for the outer screw is closer to that of curve 3.

Figure 14 shows the effect of the outer screw rotational speed on the limit pressure at the end of the solids conveying zone. According to eq. (22), the velocity of the pellets and the pressure both increase with the screw rotational speed, and this results in a higher limit pressure. As expected, centrifugal force increases with the screw rotational speed, and so does normal and tangential acceleration. These are helpful for compressing solids. Calculated pressure values are higher than experimental data because the minimum traction angle is assumed to be 0, and it is usually greater than 0.

The limit pressure implies the end of the conveying of solids, where the solids are compressed adequately so that the density is maximum. The traction angle of solids simultaneously arrives at its minimum. At this point, the drag of solids based on solid-static friction is broken down, corresponding to the appearance of a melting film. Friction coefficients, screw geometrical parameters, and screw rotational speeds all affect the limit pressure. The higher the limit pressure is, the more helpful it will be to compress solids. However, the increase in the limit pressure is not unlimited because friction heat exponentially becomes higher along the direction of the screw channel such that the melting starts. Figure 15 shows the barrel friction heat ($\dot{Q}_b$) and outer screw friction heat ($\dot{Q}_s$) along the screw-axis direction. It can be found that the interface temperature closely changes with the local pressure because of the proportional relationship between the friction heat and local pressure. When the limit pressure is high enough, the interface temperature rises to the melting point. In some sense, the limit pressure is one self-safe mechanism of a screw extruder.

CONCLUSIONS

1. One double-screw nested extruder was successfully developed for the increment of the output and capability of double-layer extrusion.
2. Compared with the output in the common combination of a stationary barrel and a rotating screw, the output increased greatly when the inner barrel and inner screw rotated oppositely for the double-extrusion systems. This was the theoretical basis for the novel extruder.
3. On the basis of the effects of centrifugal force and material compressibility, the maximum traction angle was predicted to be 90° − the helix angle for maximum output. This was in contrast to the maximum traction angle of 90° in the general opinion when the Darnell–Mol theory was used. The traction angle decreased gradually along the direction of the screw channel.
4. Acceleration and velocity as well as the acting forces could be decomposed into normal, tangential, and axial ones. The resulting normal acceleration induced the difference between the

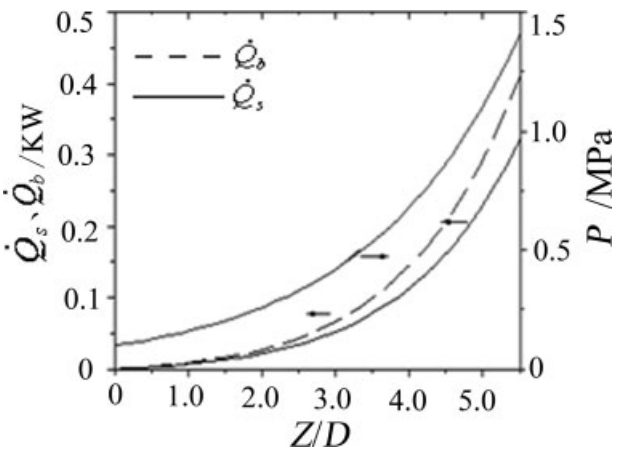

Figure 15 Pressure and friction heat along the axis direction of the outer screw.

force acting on the solids by screw and by barrel. The resultant centripetal force prevented the feeding in the case of a rotating outer screw and a stationary inner screw.

5. Minimum pressure and maximum pressure were built at the beginning and end of the solids conveying zone, corresponding to the maximum traction angle and minimum traction angle, respectively, due to centrifugal force and solid compressibility. The increment of the limit pressure was not unlimited because of the breakdown of the solid bed by the approximately exponentially increased friction heat between the solids and the metal surfaces (barrel and screw).

NOMENCLATURE

1 (subscript)	screw
2 (subscript)	barrel
A	vertical cross section area
a_a	absolute acceleration
a_c	Coriolis acceleration
a_e	convicted acceleration
a_r	relative acceleration
b (subscript)	barrel
C_0	constant
D_b	diameter of the barrel
D_s	root diameter of the screw
$\overline{dz}$	average down-channel differential increment
e	width of the screw flight
f_b, f_1	friction coefficient between the barrel and material
f_s, f_2	friction coefficient between the screw and material
H_1	channel depth
HDPE	high-density polyethylene
I_1	electric current of the outer screw
I_2	electric current of the inner screw
K	ratio of the normal stress to the axial stress
L	length of the solids conveying zone
n (superscript)	normal direction
n_1	outer screw rotational speed
N_1	normal force of the barrel acting on the solid
n_2	inner screw rotational speed
N_2	normal force of the screw acting on the solid
$\underline{p}$, P	pressure
$\overline{p}$	dimensionless characteristic parameter of the pressure
p_0	initial pressure
$\dot{Q}_b$	barrel friction heat
Q_s	volumetric flow rate of solids conveying
$\dot{Q}_s$	outer screw friction heat
s (subscript)	screw
S	screw pitch
$\underline{t}$	time
$\overline{t}$	dimensionless characteristic parameter of the pressure
t (superscript)	tangential direction
$\underline{v}$	velocity
$\overline{v}$	dimensionless characteristic parameter of the velocity
V	axial velocity
v_0	inlet velocity
$\vec{V}_a$	absolute velocity
V_b	axial velocity of the barrel
$\vec{V}_e$	convected velocity
$\vec{V}_r$	relative velocity
$\overline{W}$	average channel width
W_b	width of the channel at the barrel surface
W_s	width of the channel at the root of the screw
z (superscript)	axial direction
γ	correcting coefficient
θ	traction angle
θ_{max}	maximum traction angle
$\underline{\rho}$	material density
$\overline{\rho}$	dimensionless characteristic parameter of the density
ρ_a	material density in the atmospheric pressure
ρ_m	material density in the utmost pressure
ϕ	helix angle
$\overline{\phi}$	average helix angle
ϕ_b	helix angle of the barrel

References

1. Darnell, W. H.; Mol, E. A. J. SPE J 1959, 12, 20.
2. Chung, C. I. SPE J 1970, 26, 32.
3. Tedder, W. SPE J 1971, 27, 42.
4. Broyer, E.; Tadmor, Z. Polym Eng Sci 1972, 12, 12.
5. Fang, S. Z.; Chen, L.; Zhu, F. H. Polym Eng Sci 1991, 31, 1113.
6. Lovegrove, J. G. A.; Williams, J. G. Polym Eng Sci 1974, 14, 589.
7. Klein, I.; Klein, R. Plast Eng 1979, 10, 47.
8. Campbell, G. A.; Sweeney, P. A.; Felton, J. N. Polym Eng Sci 1992, 32, 1765.
9. Sarioglu, A.; Månson, J. A. E. Int Polym Proc 2003, 18, 219.
10. Sarioglu, A.; Hagstrand, P. O. H.; Månson, J. A. E. Polym Compos 2004, 25, 331.
11. Chung, C. I. SPE J 1956, 26, 32.
12. Qu, J. P.; Shi, B. S.; Feng, Y. H.; He, H. Z. J Appl Polym Sci 2006, 102, 2998.
13. Sun, T. H. Adv Polym Technol 1988, 8, 11.